# TREE GROWTH AND WOOD FORMATION — APPLICATIONS OF ANISOTROPIC SURFACE GROWTH

Joanne Mann*, Mike Plank† and Andy Wilkins‡

**Abstract**

A three-dimensional framework into which models of tree growth may be placed is proposed and explained by considering surface evolution of anisotropic stem-branch-obstacle systems. In order to accommodate as many different models as possible, the surface evolution law considered is quite general in that it may be dependent on time, the vector(s) describing the anisotropy, local curvatures or s'es, concentrations of growth hormones; and may be different for the stem, branches, etc. The motivation for this is to produce a framework allowing general mathematical models of tree surface growth in three dimensions to be formulated and numerically analysed. The robust, computationally stable and efficient framework for describing the evolution is based upon the fast marching method. The basic method is extended to situations where different surfaces (stem, branch, obstacle) evolve according to different growth rules, and a method for tracking the evolution of the vectors describing the anisotropy is detailed. This anisotropy (the wood's grain) is modelled using an incompressible fluid and explicit solutions are found for the situation where the stem contains a dead branch, and for the region around a live branch–stem junction.

The evolution of curves in two dimensions is also explored analytically to provide insight into the more complicated 3D case. Explicit formulae valid for any evolution law are given for the evolution of: distances along the curve; the local curvature; and the average magnitude of the curvature. Two-dimensional analogues of tree growth past obstacles with curvature- and hormone-driven growth are solved analytically and display expected characteristic behaviours.

The results of the numerical simulations are visualised using MATLAB. Three cases are tested: a stem with a cluster of 5 branches; the growth of a stem around

*Institute of Information and Mathematical Sciences, Massey University Auckland, Albany, Private Bag 102 904, North Shore Mail Centre, NZ. Email j.l.mann@massey.ac.nz
†Mathematics and Statistics Department, University of Canterbury, Private Bag 4800, Christchurch, NZ. Email M.Plank@math.canterbury.ac.nz
‡Department of Mathematics, University of Queensland, Brisbane Q4072, Australia. Email awilkins@maths.uq.edu.au

an obstacle; and a combination of these two with different growth rates for the stem and branches.

# 1. Introduction and Outline

## 1.1. General introduction

Ensis is a joint venture between Scion (New Zealand Forest Research Institute) and Australia's CSIRO Forestry and Forestry Products. Rapidly producing trees containing timber with large sections of straight, uniform grain, uninterrupted by knots or branches, is one of a forester's main goals. This is aided by mathematical models of tree growth, which range from macroscopic empirical models down to microscopic physiological models (see [13] for an example). However, the Ensis representatives realised that none of the mathematical models proposed have been set in a three dimensional context, chiefly because of a lack of a known general mathematical framework into which to place them.

The problem that the Ensis' representatives presented was *to develop a robust framework for describing growing surfaces which may be anisotropic*. This framework should:

- be numerically stable under any physically-reasonable local evolution law;
- have the ability to track in time any vector(s) describing the local anisotropy;
- be applied in a few simple examples, for instance a stem with a single branch;
- be able to be applied to growth of a tree's surface as well as cell-wall thickening;
- include a visualisation component.

Concurrently, the MISG team should consider the mathematical modelling of growing trees and wood cells, bearing in mind the literature for tree growth is enormous (some references are [6, 7, 9, 10, 13, 17, 18]).

It became apparent during the course of MISG2006 that, due to a lack of experimental observations, it would be impossible to build a useful model of cell expansion and cell-wall thickening, so the team concentrated on macroscopic tree growth. Only growth in the girth of stems and branches was considered, since height/length growth was considered beyond the scope of this project. Finally, the experimental observations may be more relevant to pinus radiata than to other trees.

## 1.2. Mathematical remarks

The problem may therefore be summarised as follows. Every point on the tree's surface, $\mathbf{r}$ (a 3-vector), is equipped with a unit normal $\mathbf{n}$, and a special tangent direction, $\mathbf{g}$, which points along the direction of the grain ($\mathbf{n} \cdot \mathbf{g} = 0$). The evolution law in time ($t$) is

$$\frac{\mathrm{d}\mathbf{r}}{\mathrm{d}t} = v\mathbf{n} \ , \tag{1}$$

where the "velocity function", $v$, may be dependent on $t$, $\mathbf{g}$, the local curvatures or stresses, whether the point in question is part of the stem or a branch, concentrations of growth hormones, etc. This is shown in Figure 1.

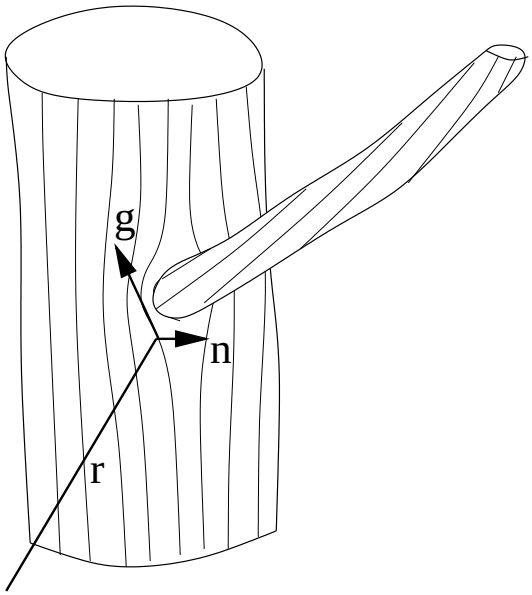


*Figure 1.* A stem with a single branch. The grain is shown as well as an example normal (out of page in this case), $\mathbf{n}$, and grain direction, $\mathbf{g}$ directions.

Equation (1) is deceptively simple. Although possible, it may be inconvenient to parameterise the surface and embed into $\mathrm{R}^3$ using a function $\mathbf{r}$. Moreover, in many instances the surface evolution may be frustrated by "shocks", or regions where two surface patches are growing into each other (such as the conflict between the stem and the upper surface of an upwards-tilting branch), and the numerical implementation must be able to handle this. The level set and fast marching methods [15] handle both of these problems naturally.

The evolution of **g** is discussed below in Sections 5 and 6.
Reiterating, the problem brought to MISG reduces to:

1 implement a numerically stable algorithm to evolve the surface under equation (1) with any $v$, apply it for a few simple initial configurations and visualise it;

2 investigate some mathematical models that yield realistic $v$.

## 1.3. Outline

A number of experimental observations were presented to the team by the Ensis representatives. These are summarised in Section 2.

Section 3 contains general remarks about curvature-driven growth, and analytic calculations concerning growth of "surfaces" in 2D, both curvature-driven and driven by hormones. Explicit formulae valid for any evolution law in 2D are given for the evolution of distances along evolving curves, and also the evolution of curvature and "total variation" along such curves. These results and the examples worked through should prove a useful guide for future studies involving modelling the growth velocity.

Section 4 details a stable, efficient numerical method — the fast marching method — for tracking the growth of an isotropic surface. This method is also extended to the case where the stem and branches of the tree are evolving according to different growth rules.

In Section 5 the problem of determining grain direction is considered. The literature is quite sparse on this subject, but in one model [6, 8] the grain is thought of as streamlines of an incompressible fluid running from the leaves to the roots. This yields qualitatively realistic grain patterns. Two examples are worked through: that of a dead branch attached to a stem; and, a live branch attached to a stem.

Section 6 outlines a model for including grain direction in the fast marching method, and hence tracking the evolution of an anisotropic surface.

Finally, in section 7, the method of visualising the output of the numerical methods is described and the results of simulating tree growth in three dimensions are presented and discussed.

Appendix 8 contains a table of the mathematical notation.

# 2. Experimental observations of tree growth

The Ensis representatives requested that it should be possible to include the following experimental observations [2, 3, 4] concerning the velocity, $v$, and grain direction, **g**, in the framework. A book that has

general information regarding trees is [9]. Many of the following experimental observations may be seen in evidence in the cross-sectional photograph in Figure 2

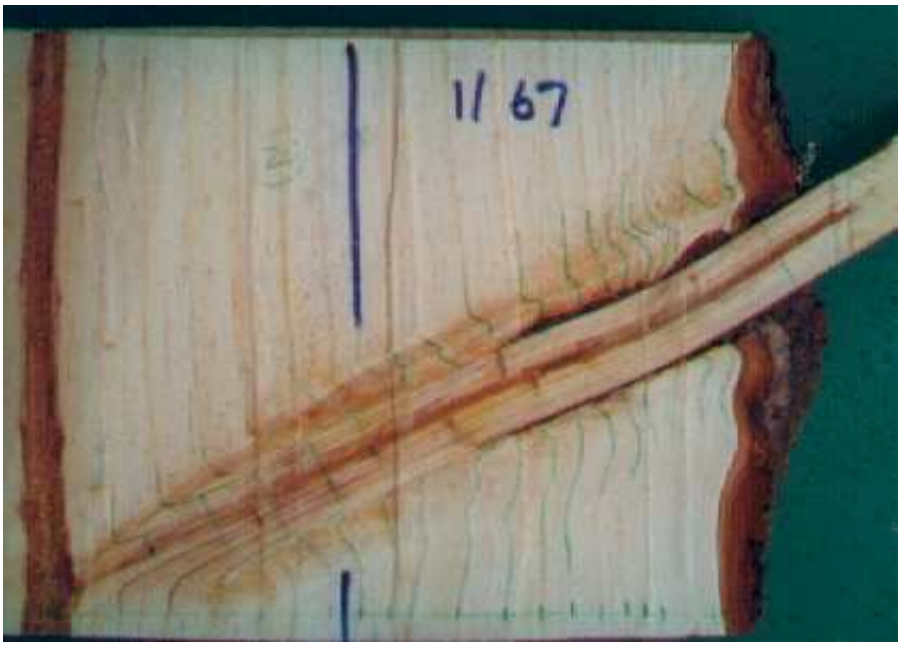


*Figure 2.* A cross-section of pinus radiata stem with one branch. The left-hand edge is the core (pith) of the stem. This sample shows time-dependent growth, the concave/convex patterns around junctions, the death of the branch, and the grain running into the branch.

## 2.1. Growth with time

An isolated stem or branch appears to grow with $v = v(t)$ in a manner similar to the sketch of Figure 3. The functional form of $v(t)$ may be readily obtained from experiment.

## 2.2. Growth of young branches

A complicated pattern of convex and concave regions of wood surrounds the branch-stem joint, as shown in Figure 4. The convex/concave regions are roughly symmetric around the axis of the branch. After a few years of growth they disappear.

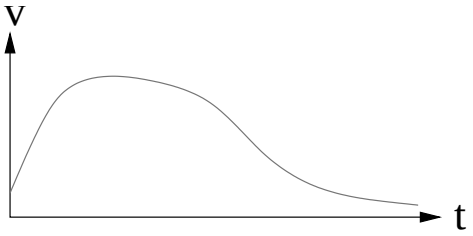


*Figure 3.* A sketch of the velocity, $v$, as a function of time, $t$, for an isolated stem or branch.

## 2.3. Death of branches

Branches grow for a few years and then cease growing, often dying. Conversely, the stem continues to grow. This means that

$$v_{\text{stem}} \neq v_{\text{branch}} \ .$$

This may be seen in Figure 4.

## 2.4. Grain

Grain may be approximately straight in the direction of the stem/branch axis, or it may be 'spiral grain' which follows a helix around the axis. The pitch of spiral grain often varies from year to year. It is not uncommon for a left-handed helix to gradually change into a right-handed version (or vice-versa) over the course of about 20 years. According to the Ensis representatives, it is atypical for the grain to change chirality more than once in the life of a tree.

Interestingly, recent research [2] contradicts the conventional wisdom [16] concerning grain patterns around stem-branch junctions. The recent research suggests that grain runs down the axis of a branch and then runs down, *not* up the stem, and that grain appears to be contiguous to the stem-grain only in a first few years of a branch's life. After these first years, and corresponding approximately with the death of the branch, the grain in the stem runs around the branch, treating it like an obstacle.

## 2.5. Removal of branches and growth around obstacles

Often dead branches are broken or pruned off the stem. This can be beneficial for the tree for it effectively allows the branchless part of the stem to be taller. The stem grows around the remaining branch-stub and eventually completely encases it. Occasionally trees encounter

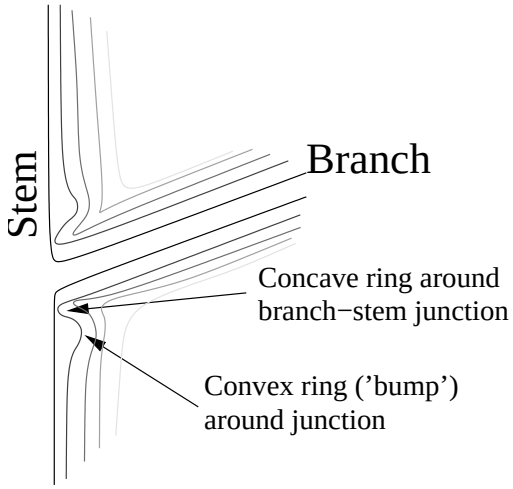


*Figure 4.* A cross-sectional sketch of the time sequence of the region around a stem-branch junction. Blacker lines: early times. Whiter lines: late times. There is a pronounced concave ring around the base of the branch, and further out on the stem there is a circular swelling, called here the "bump". At later times these concave/convex regions disappear.

obstacles (such as fences) and grow around these obstacles in the same way. A typical time sequence is shown in cross section in Figure 5, and photographs can be found in [9].

## 3. Some analytic calculations

Curvature-driven and hormone-driven growth are discussed in this section. Firstly, some general remarks are made concerning curvature-driven growth and it is argued that it is likely to be irrelevant for tree growth. Nevertheless, because it is so common in surface-growth problems, a summary of the mathematics of curvature is given. Explicit formulae are derived for the evolution of a space curve in 2D; the evolution of the distance (metric) along such a curve; the evolution for the curvature of the curve; and the evolution of the average value of the magnitude of its curvature in 2D: all for a completely general evolution law. A problem that is analytically solvable is presented, because this should provide insight into more realistic problems which are only solvable numerically. It is an attempt to model the "bump" occurring in Figures 4 and 5. Finally, a hormone-driven growth problem is solved, again not because it is perfectly realistic, but because it should provide a feel for the types of behaviours manifested by this type of growth.

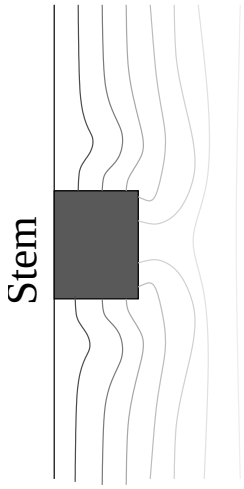


*Figure 5.* Growth around an obstacle (shaded) — cross-section of tree. Blacker lines: earlier times. Whiter lines: later times. A definite "bump" is seen, similar to that of Figure 4, but experimental evidence was not detailed enough to determine whether there is also a "concave region". The stem grows over the obstacle, producing knuckle-like surfaces before completely enclosing the obstacle.

## 3.1. Curvature-driven growth

In other areas involving the growth of surfaces, such as flame fronts or crystal growth [15], it is common for the velocity to be dependent on the local curvature, $\kappa$. For example, the velocity may be assumed to be a linear function

$$v = a + b\kappa \ . \tag{2}$$

It is unclear whether this is pertinent for tree growth, since tree growth is not a crystallization process, and dimensional arguments suggest $v = a$ is more likely. Let us speculate further.

One simple assumption is that a surface area, $A$, of tree produces a volume of material $vA\Delta t$ in time $\Delta t$, where $v$ is a proportionality constant parameterising the speed of wood deposition. The units of $v$ are m/s, and it is evidently the velocity found in equation (1). The simplest assumption is that $v$ is constant ($v = a$) but in a more elaborate treatment we would account for curvature effects by *expanding around the planar situation* in a power series:

$$v = a(1 + \tilde{b}\kappa + O(\kappa^2)) \ .$$

However, this means that $\tilde{b}$ has the dimensions of length, since $\kappa$ has dimension of 1/length. It is unclear what this parameter would be save

for a microscopic parameter such as the typical diameter or length of a wood cell, or even the length/diameter of a macromolecule in the cell. These are all very small, so their product with $\kappa$ in the term $\tilde{b}\kappa$ would lead to an insignificant correction to the simple law $v = a$ for all but the most severe curvatures.

The same arguments can be made concerning the curvature of the grain: one proposition is that curved grain (such as spiral grain or grain around a branch-stem joint) may result in different growth characteristics than straight grain, viz., perhaps $v = a+b\kappa$, where $\kappa$ is the curvature of the grain. However, $b$ should contain some length parameter, which would probably be the cell diameter, or possibly the cell length, both of which yield an insignificant $b\kappa$.

In contrast, flame propagation and crystalization have been modelled using curvature-dependent growth. These are rather different phenomena, however: flame propagation in a combustible mixture depends on thermal and mass diffusion and the thickness of the flame front, which all provide suitable length scales; while the rate of crystal growth into a solution phase depends on the available sites for molecular attachment which in turn depends on the length scales of defects in the crystal and the molecular sizes. The existance of these natural length scales makes curvature-dependent growth more plausable.

Of course, the arguments concerning tree growth are purely hypothetical since it is likely that the rate of material deposition is not proportional to the tree's surface area. Moreover, it may also be true that the length of fibres does correlate with the growth rate of trees, and it is not uncommon in anatomy to find genetically determined length scales that emerge after morphogenesis (an early paper is [19]). Finally, the very fact that the cambium is fairly smooth and cylindrical indicates that the growth tends to discourage any local increases in curvature, so that $v = a + b\kappa$ with $a > 0$ and $b < 0$ (but small) may be appropriate in some microscopic models where curvatures on the scale of cells play a role. Therefore, we summarise some results concerning the curvatures of space curves and surfaces.

There are many online references describing curvatures of space curves and surfaces, see for example [20, 21, 22], and Sections 3.1.2 and 3.1.3 contain a collection of the most useful formulae, without proof.

**3.1.1 Qualitative curvature-driven growth.** Curvature-driven growth under $v = a + b\kappa$ can either accentuate or dampen the effects of high-curvature regions, as may be seen in Figure 6, depending on the sign of $b$.

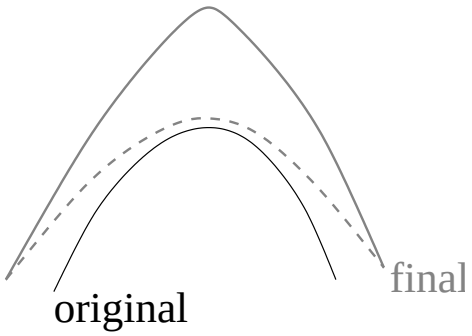


*Figure 6.* Curvature driven growth from an original (lower) surface to final (upper) surfaces under $v = a + b\kappa$. The solid final surface has $a > 0$ and $b > 0$. The dashed final surface has $a > 0$ and $b < 0$.

**3.1.2 Curvature and torsion of space curves.** A space curve is simply a 1-dimensional curve lying in 2 or 3 dimensional space. It may be parameterised by $\xi$ which increases monotonically along the curve, and can be embedded in 2D or 3D using $\mathbf{r}(\xi)$. Its curvature, $\kappa$, and torsion, $\tau$, may be calculated through the relations

$$\kappa(\xi) = \frac{|\mathbf{r}' \times \mathbf{r}''|}{|\mathbf{r}'|^3} \quad \text{and} \quad \tau(\xi) = \frac{|\mathbf{r}' \cdot \mathbf{r}'' \times \mathbf{r}'''|}{|\mathbf{r}' \cdot \mathbf{r}''|^2} \ ,$$

where the prime denotes differentiation with respect to $\xi$.

- The *curvature* at a point is the reciprocal of the radius of curvature of a circle which most closely matches the space curve at that point (the so-called 'osculating circle').

- The *torsion* determines how out-of-plane the curve is, and is zero for a curve lying in a plane, positive for a right-handed helix, and negative for a left-handed helix.

In principle, the velocity, $v$, could be a function of both curvature and torsion of the grain.

The unit tangent vector is

$$\mathbf{T} = \frac{\mathbf{r}'}{|\mathbf{r}'|} \ .$$

Derivatives of it can be expressed in terms of the unit normal and binormal via the classical Frenet formulae [21]:

$$\begin{aligned} \mathbf{T}' &= |\mathbf{r}'|\kappa\mathbf{N} \ , \\ \mathbf{N}' &= -|\mathbf{r}'|\kappa\mathbf{T} + |\mathbf{r}'|\tau\mathbf{B} \ , \\ \mathbf{B}' &= -|\mathbf{r}'|\tau\mathbf{N} \ . \end{aligned}$$

If $\xi$ is the arc-length then $|\mathbf{r}'| = 1$ and these formulae simplify somewhat.

**3.1.3 Curvatures of surfaces.** There are a number of useful measures of curvature at a point on a 2D surface embedded in 3D.

The *principal curvatures* are calculated by considering curves on the surface going through a point. Denote the unit normal to the surface by $\mathbf{N}$, and let $\mathbf{v}$ be a unit tangent vector. Consider the curve produced by the intersection of the surface with the plane defined by $\mathbf{N}$ and $\mathbf{v}$. It will have zero torsion, and by the second Frenet formula (above), the curvature at the point is $|\nabla_v \mathbf{N}|$ (with $\nabla_v = \mathbf{v} \cdot \nabla$). The maximum and minimum of these curvatures (choosing all possible $\mathbf{v}$) are called the principal curvatures, $k_1$ and $k_2$.

The *Gaussian curvature* at a point on a surface is the product of the principal curvatures, $k_1 k_2$ (or $\det \nabla_v \mathbf{N}$). Imagine an ant tied to the point with a short thread of length $r$. The ant runs around the point while the thread is completely stretched and measures the length $L(r)$ of one complete trip. If the surface were flat, $L(r) = 2\pi r$. Using the measured length, the Gaussian curvature can be calculated through the formula

$$\text{Gaussian curvature} = \lim_{r \to 0} \frac{3(2\pi r - L(r))}{\pi r^3} \ .$$

The Gaussian curvature has units of length$^{-2}$.

The *mean curvature* at a point on a surface is the mean of the principal curvatures, $(k_1 + k_2)/2$ (or $\frac{1}{2}\mathrm{tr}\, \nabla_v \mathbf{N}$). It may also be calculated by constructing the unit normal to the surface, $\mathbf{N}$, and taking its divergence:

$$\text{mean curvature} = \nabla \cdot \mathbf{N} \ .$$

The mean curvature has units of length$^{-1}$.

## 3.2. Curvature-driven growth in 2D

Let $\mathbf{r}(\xi, t) = (x(\xi, t), y(\xi, t))$ denote the position vector in $R^2$. We consider a family of curves generated by an initial curve $\gamma(0)$ described by $\mathbf{r}(\xi, 0)$, $\xi \in [\xi_0, \xi_1]$, under the condition that the evolution velocity along the normals is a function of curvature. The situation is shown in Figure 7.

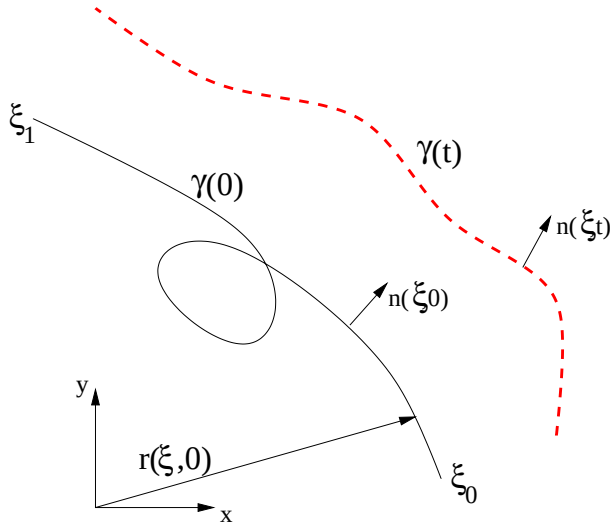


*Figure 7.* An initial curve (solid), $\gamma(0)$, and a curve at a later time (dashed), $\gamma(t)$. The curves are parameterised by $\xi$ (not necessarily arclength, but monotonically increasing from $\xi_0$ to $\xi_1$), and embedded into $R^2$ with $\mathbf{r}(\xi, t)$. Two unit normals are depicted. We also introduce the standard Cartesian coordinates $(x, y)$ as shown.

**3.2.1 Equations in Cartesian coordinates.** The family of curves parametrized by $t$ evolves according to the partial differential equation (1):

$$\mathbf{r}_t(\xi, t) = v\left(\kappa(\xi, t)\right) \mathbf{n}(\xi, t) \ .$$

The subscript notation is a shorthand for differentiation, for example,

$$\mathbf{r}_t \equiv \frac{\partial \mathbf{r}}{\partial t} \quad \text{and} \quad \mathbf{r}_\xi \equiv \frac{\partial \mathbf{r}}{\partial \xi} \ .$$

In Cartesian coordinates, the unit normal is

$$\mathbf{n}(\xi, t) = \frac{(y_\xi, -x_\xi)}{\sqrt{y_\xi^2 + x_\xi^2}} \ ,$$

and the above formulae give

$$\kappa(\xi, t) = \frac{y_{\xi\xi} x_\xi - x_{\xi\xi} y_\xi}{\left(x_\xi^2 + y_\xi^2\right)^{3/2}} \ .$$

Hence, equation (1) can thus be recast as the system

$$\begin{aligned} x_t &= \frac{v(\kappa)y_\xi}{\sqrt{x_\xi^2 + y_\xi^2}} \ , \\ y_t &= \frac{-v(\kappa)x_\xi}{\sqrt{x_\xi^2 + y_\xi^2}} \ , \end{aligned}$$

valid in 2D.

Finally,

$$|\mathbf{r}_t| = |v(\kappa)|\,|\mathbf{n}| = |v(\kappa)| \ ,$$

so that $|v(\kappa)|$ is truly the "speed" of the curve evolution along the normal.

**3.2.2 The curve metric.** The family of curves $\gamma(t)$ and the family of curves $\beta(\xi)$ defined by $\mathbf{n}(\xi, t)$, $t \in [0, t_1]$ can be regarded as an orthogonal coordinate system for a portion of the plane,

The metric corresponding to this coordinate system is given by

$$\mathrm{d}s^2 = E\ \mathrm{d}\xi^2 + 2F\ \mathrm{d}\xi\ \mathrm{d}t + G\ \mathrm{d}t^2 \ , \tag{3}$$

where

$$\begin{aligned} E &= \mathbf{r}_\xi \cdot \mathbf{r}_\xi \ , \\ F &= \mathbf{r}_\xi \cdot \mathbf{r}_t = 0 \ , \\ G &= \mathbf{r}_t \cdot \mathbf{r}_t = v^2(\kappa) \ . \end{aligned}$$

We can call the function $E$ the *curve metric* because the arclength, $a$, along $\gamma$ is given by

$$\mathrm{d}a = \sqrt{E}\mathrm{d}\xi \ .$$

Hence $\sqrt{E}$ is related to measuring distances along the curve $\gamma$.

**3.2.3 Evolution of the curve metric.** It is of interest to derive the evolution law for the curve metric since this gives a direct handle on the evolution of distances between points on the curve. Now,

$$E_t = 2\mathbf{r}_\xi \cdot \mathbf{r}_{\xi t} \ ,$$

and since $\mathbf{r}_t \cdot \mathbf{r}_\xi = 0$,

$$(\mathbf{r}_t \cdot \mathbf{r}_\xi)_\xi = \mathbf{r}_{\xi t} \cdot \mathbf{r}_\xi + \mathbf{r}_t \cdot \mathbf{r}_{\xi\xi} = 0 \ ;$$

hence

$$E_t = -2\mathbf{r}_t \cdot \mathbf{r}_{\xi\xi} \ .$$

Substitution of equation (1) yields

$$E_t = -2v(\kappa)\mathbf{n}\cdot\mathbf{r}_{\xi\xi} \ ,$$

and since

$$\mathbf{n}\cdot\mathbf{r}_{\xi\xi} = \frac{x_{\xi\xi}y_\xi - x_\xi y_{\xi\xi}}{\sqrt{E}} = -E\kappa \ ,$$

we have

$$\frac{\partial E}{\partial t} = 2v(\kappa)E\kappa \ , \tag{4}$$

which is the equation governing the evolution of distances, $E$, along the space curve.

**3.2.4 Evolution of the curvature.** Similarly, an expression for the evolution of the curvature may be derived.

The coordinate system lies in the plane and hence the Gaussian curvature produced by the metric (3) must be zero. For orthogonal coordinates, the Gaussian curvature $K$ is given by

$$\text{Gaussian curvature} = -\frac{1}{2\sqrt{EG}}\left\{\frac{\partial}{\partial t}\left(\frac{E_t}{\sqrt{EG}}\right) + \frac{\partial}{\partial \xi}\left(\frac{G_\xi}{\sqrt{EG}}\right)\right\} \ ,$$

and, since this is zero, we have

$$\frac{\partial}{\partial t}\left(\frac{E_t}{\sqrt{EG}}\right) = -\frac{\partial}{\partial \xi}\left\{\frac{G_\xi}{\sqrt{EG}}\right\} \ .$$

In terms of $E$, $v$ and $\kappa$, this becomes

$$\frac{\partial}{\partial t}\left(\frac{E_t}{\sqrt{E}v}\right) = -\frac{\partial}{\partial \xi}\left\{\frac{2v_\xi}{\sqrt{E}}\right\} \ , \tag{5}$$

while the evolution for the curve metric (4) implies

$$\frac{E_t}{\sqrt{E}v} = 2\sqrt{E}\kappa \ ;$$

consequently, equation (5) becomes

$$\frac{\partial}{\partial t}(\sqrt{E}\kappa) = -\frac{\partial}{\partial \xi}\left\{\frac{v_\xi}{\sqrt{E}}\right\} \ .$$

Using the evolution law for the curve metric, this equation can be recast as

$$\frac{\partial \kappa}{\partial t} = -\frac{1}{\sqrt{E}}\frac{\partial}{\partial \xi}\left\{\frac{v_\xi}{\sqrt{E}}\right\} - v\kappa^2. \tag{6}$$

Although derived differently, equations (4) and (6) are in agreement with the equations (2.7) and (2.8) in Sethian's paper [14]. These equations form the "backbone" of much of his analysis.

Equation (6) can be simplified by a change in variable that corresponds to replacing $\xi$ with arclength along the curve. Arclength, $a$, is defined above ($\mathrm{d}a = \sqrt{E}\mathrm{d}\xi$), with

$$\frac{\partial}{\partial \xi} = \frac{1}{\sqrt{E}} \frac{\partial}{\partial a} \ .$$

Equation (6) thus simplifies to

$$\frac{\partial \kappa}{\partial t} = -\frac{\partial^2 v}{\partial a^2} - v\kappa^2. \tag{7}$$

This is the most convenient form to analyse the evolution of the curvature, $\kappa = \kappa(\xi, t)$, under various evolution laws.

**3.2.5 The total variation.** A conspicuous quantity that is studied in the theory of evolving wavefronts is the total variation $\Lambda(t)$ of a curve $\gamma(t)$. It is the average value of $|\kappa|$ along the curve, multiplied by the length of the curve. Mathematically:

$$\Lambda(t) = \int_{\xi_0}^{\xi_1} |\kappa| \sqrt{E} \ \mathrm{d}\xi \ ; \tag{8}$$

it represents an "energy-like" quantity. Indeed, this is the quantity that commands the attention of Sethian's [14] analysis of wavefronts. The p.d.e. (6) can be used to express the rate of change of $\Lambda$ in terms of the terminal curvatures and derivatives of $\gamma(t)$.

In order to expedite the mathematics, assume $\kappa \geq 0$; hence

$$\frac{\mathrm{d}\Lambda}{\mathrm{d}t} = \int_{\xi_0}^{\xi_1} \frac{\partial}{\partial t} \kappa \sqrt{E} \ \mathrm{d}\xi = \int_{\xi_0}^{\xi_1} \left( \kappa_t \sqrt{E} + \frac{\kappa}{2\sqrt{E}} E_t \right) \ \mathrm{d}\xi \ .$$

Equations (4) and (6) give

$$\begin{aligned} \frac{\mathrm{d}\Lambda}{\mathrm{d}t} &= \int_{\xi_0}^{\xi_1} \left( -\frac{1}{\sqrt{E}} \frac{\partial}{\partial \xi} \left\{ \frac{v_\xi}{\sqrt{E}} \right\} - v\kappa^2 \right) \sqrt{E} + \frac{\kappa}{2} \sqrt{E} \, 2v\kappa \Bigg) \ \mathrm{d}\xi \\ &= \int_{\xi_0}^{\xi_1} -\frac{\partial}{\partial \xi} \left\{ \frac{v_\xi}{\sqrt{E}} \right\} \ \mathrm{d}\xi \ , \end{aligned}$$

so that

$$\frac{\mathrm{d}\Lambda}{\mathrm{d}t} = -\frac{\mathrm{d}v}{\mathrm{d}\kappa} \frac{\kappa_\xi}{\sqrt{E}} \Bigg|_{\xi_0}^{\xi_1} \ , \tag{9}$$

which is the evolution law for $\Lambda$.

It is immediately obvious that for closed curves

$$\frac{\mathrm{d}\Lambda}{\mathrm{d}t} = 0 \ ,$$

irrespective of the evolution law, $v$, so the average value of $|\kappa|$ is inversely proportional to the length of the curve.

**3.2.6 A final example.** Consider the case where the curve lying in 2D is parameterised by by $y = y(x,t)$ (that is, consider the special case $x = \xi$ in the above). This is depicted in Figure 8. The slope angle, $\phi$, is given by

$$\tan\phi = \partial_x y \ ,$$

where $\partial_x = \partial/\partial x$ indicates a partial derivative. Using the formula given above, the curvature is

$$\kappa = \frac{\partial_x^2 y}{(1+(\partial_x y)^2)^{3/2}} \ .$$

At a point with slope angle $\phi$, shifting the surface by a small displacement in the normal direction, $\mathrm{d}N$, induces a corresponding shift, $\mathrm{d}y$, in $y$. These shifts are clearly related by

$$\mathrm{d}N = |\cos\phi|\mathrm{d}y \ ,$$

as may be seen in Figure 8 (note that $\phi \in (-\pi/2, \pi/2)$). Taking the derivative with respect to $t$ gives

$$\frac{\partial N}{\partial t} = |\cos\phi|\frac{\partial y}{\partial t} = \frac{1}{\sqrt{1+\tan^2\phi}}\frac{\partial y}{\partial t} = \frac{1}{\sqrt{1+(\partial_x y)^2}}\frac{\partial y}{\partial t} \ .$$

Thus, the equation $\mathrm{d}N/\mathrm{d}t = a + b\kappa$ becomes

$$\frac{\partial y}{\partial t}\frac{1}{\sqrt{1+(\partial_x y)^2}} = a + b\frac{\partial^2 y}{\partial x^2}\frac{1}{(1+(\partial_x y)^2)^{3/2}} \ . \tag{10}$$

It would be nice if this model could reproduce the "bump" shown in Figures 4 and 5. A potential situation where this might occur is when the surface is "pinned" by an obstacle at $x = 0$. Specifically, consider the case where $y = 0$ at $t = 0$, that is, the surface is evolving from a straight line. Then pin the point at $x = 0$, i.e., fix $y = 0$ at $x = 0$ for all $t$ and demand that $y \to at$ as $x \to \infty$. This kind of situation is drawn in Figure 9 (the particular solutions graphed are for the model in the next section).

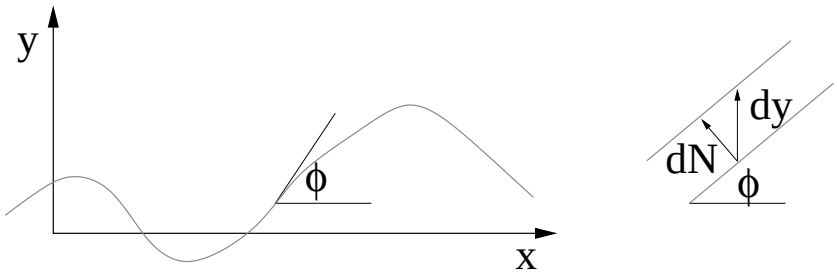


*Figure 8.* An analogue of a surface is a function $y = y(x)$, represented by the grey curve. The angle $\phi$ is shown.

Equation (10) appears difficult to solve, however, $1 + (\partial_x y)^2$ may be replaced by $(1 + \partial_x y)^2$ when $|\partial_x y|$ is very small (both expressions are unity), or very large (both expressions are $(\partial_x y)^2$). Then introduce $u(x,t) = y(x,t) + x$, and the equation to be solved reads

$$\partial_t u = a|\partial_x u| + b\partial_x^2 u/(\partial_x u)^2 \ .$$

An implicit solution may be found by considering $x = x(u,t)$ to be the dependent variable. Then using the identity

$$\partial_t x \partial_u t \partial_x u = -1 \ ,$$

(the RHS is negative), the equation for $x$ reads

$$\partial_t x = -a + b\partial_u^2 x \ ,$$

when $\partial_x u > 0$, i.e., $\partial_x y > -1$. The boundary conditions become $x(u,0) = u$; $x(0,t) = 0$; and $x \to u - at$ as $u \to \infty$.

The solution may be obtained through the use of standard but lengthy manipulations involving Laplace transforms, and may be verified (via substitution into the DE) to be

$$x = u - at + a\int_0^t \mathrm{erfc}\left(\frac{u}{2\sqrt{bt_1}}\right) \mathrm{d}t_1 \ ,$$

where erfc is the complimentary error function:

$$\mathrm{erfc}\,(z) = 1 - \frac{2}{\sqrt{\pi}}\int_0^z e^{-z_1^2}\mathrm{d}z_1 \ .$$

This erfc function is exponentially close to zero for large positive arguments, but $\mathrm{erfc}(0) = 1$.

The important conclusion is that when $y$ is reintroduced via $y = u - x$, the derivative $\partial_u y \neq 0$ except for $t = 0$:

$$\partial_u y = -\frac{2}{\sqrt{\pi}} \int_0^t e^{-u^2/\sqrt{4bt_1}} \frac{1}{2\sqrt{bt_1}} \mathrm{d}t_1 \ .$$

Thus there is no local maximum — there is no "bump". This may be due to the simplification $1 + (\partial_x y)^2 \to (1 + \partial_x y)^2$, the particular boundary conditions explored (trees may not display "bumps" in these situations), or the model may not be elaborate enough. The numerical solutions presented in later sections do display "bumps", however,

A similar model, which prescribes the slope, $\partial y/\partial x$, at the boundary $x = 0$ is solved in [1].

## 3.3. Hormone-driven growth

A different kind of structure may be obtained from equation (10) by introducing an additional growth term proportional to concentration, $C(x,t)$, of a growth hormone:

$$\frac{\partial y}{\partial t} \frac{1}{\sqrt{1 + (\partial_x y)^2}} = a + kC(x,t) + b \frac{\partial^2 y}{\partial x^2} \frac{1}{(1 + (\partial_x y)^2)^{3/2}} \ .$$

This is difficult to solve analytically, so instead a variant of it is studied:

$$\partial_t y = a + kC(x,t) + b\partial_x^2 y \ . \tag{11}$$

As will be seen, $\partial_x y$ is small for $x \gg 0$, while for the other region, $x \sim 0$, the solution is constrained by the boundary conditions. Therefore, it is hoped that this simpler equation displays similar behaviour to the more complicated model.

The boundary conditions are those of the previous section where there is an obstacle positioned at $x \leq 0$ and the key simplifying assumption is that wood cells are necrotic when compressed against this obstacle. So, for $y = y(x,t)$,

$$y(x,0) = 0 \quad \text{and} \quad y(0,t) = 0 \quad \text{and} \quad \lim_{x \to \infty} y(x,t) = at \ .$$

For illustration purposes, assume that growth hormone is released in the neighbourhood of $x = 0$ over a time which is short compared to the response times for wood growth. The hormone then diffuses to $x > 0$, and the concentration may be approximated by the solution to the linear diffusion equation:

$$C(x,t) = q_0 t^{-1/2} \exp\left(-\frac{x^2}{4Dt}\right) \ ,$$

where $q_0$ is a proportionality constant and $D$ is the diffusivity.

Equation (11) with this concentration may be solved using standard but somewhat lengthy manipulations involving Laplace transforms. The particular solution may be verified to be

$$\begin{aligned} y_{\text{partic}} &= \frac{kq_0\sqrt{\pi}}{1-b/D} f_{\text{partic}}(D) \quad \text{with} \quad f_{\text{partic}}(D) \\ &= 2\sqrt{\frac{t}{\pi}} \exp\left(-\frac{x^2}{4Dt}\right) - \frac{x}{\sqrt{D}} \text{erfc}\left(\frac{x}{2\sqrt{Dt}}\right) , \end{aligned}$$

where erfc is the complementary error function. The solution which obeys the boundary conditions is

$$y = at + \frac{kq_0\sqrt{\pi}}{1-b/D} \left(f_{\text{partic}}(D) - f_{\text{partic}}(b)\right) - a \int_0^t \text{erfc}\left(\frac{x}{2\sqrt{bt'}}\right) \mathrm{d}t' .$$

This displays the expected behaviour, as shown in Figure 9

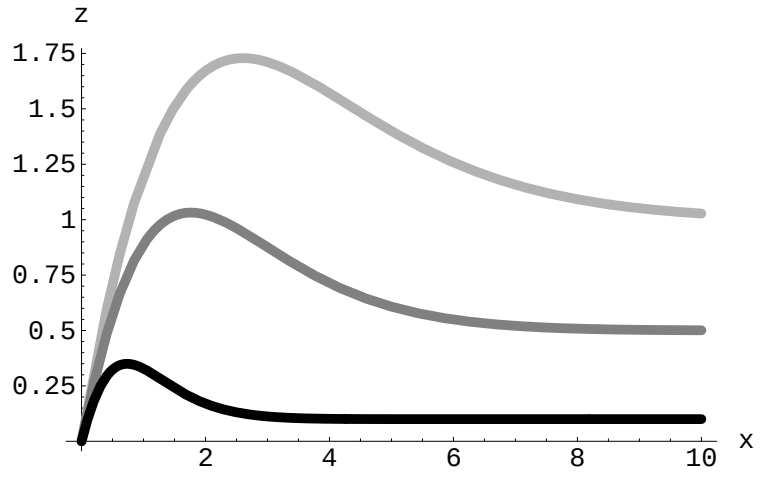


*Figure 9.* The surface of a tree growing upwards in time (black $t = 0.1$, dark grey $t = 0.5$, light grey $t = 1.0$) with the parameters $kq_0 = 1$, $a = 1$, $b = 2$, $D = 10$. Because the hormone is initially released at $x = 0$ and then diffuses to $x > 0$, a 'bump' appears as in Figures 4 and 5.

## 4. Fast marching method for an isotropic surface

Traditional numerical methods for solving surface evolution equations of the form (1) often approximate the position of the surface at a given point in time using a set of marker particles, and then move the particles

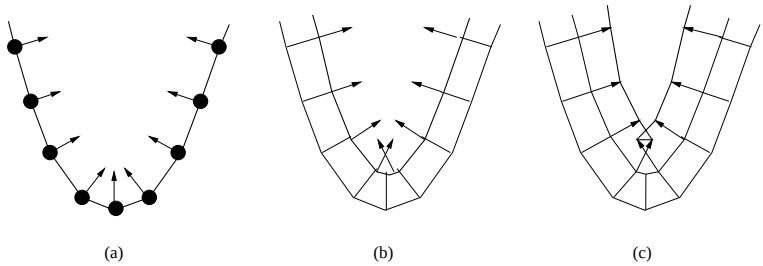


*Figure 10.* Representation of a surface moving with constant velocity using marker particles (a). A shock forms in the concave part of the surface (b), leading to formation of a closed loop and breakdown of the numerical method (c).

according to the equations of motion. Such methods, known as marker particle or nodal methods, have a number of major disadvantages. The most significant of these is that, if two particles grow close to one another, the discretised equations become highly sensitive to numerical errors in their positions, leading to an unstable aggregation of small errors. This necessitates some kind of smoothing of the particle positions, or redistribution of particles evenly along arc length, neither of which is desirable from a numerical point-of-view. Furthermore, nodal methods will typically break down if a shock develops in the surface. This can occur, for example, in a concave region of a surface evolving with a velocity function of the form (2) with $b \geq 0$ (see Figure 10). Particles on either side of the shock cross paths, forming a closed loop in the interface, which must be removed to maintain the correct position of the surface (which may be viewed as a weak solution of the governing equations). This "de-looping" may be achieved by deleting appropriate particles as the surface moves, but this is extremely difficult to achieve for a three-dimensional problem.

An alternative approach is to represent the surface implicitly, as the level surface of some function. This may be done in one of two ways: the surface at time $t$ may be embedded as the zero level set of a function $\phi(\mathbf{x}, t)$; or as the level set $T = t$ of a function $T(\mathbf{x})$, which is the *time of arrival* of the surface at the point $\mathbf{x}$. The former approach leads to an initial value problem for $\phi$, whilst the latter results in a boundary value problem for the arrival time function $T$. The main practical difference between the two systems is that the latter can only describe surfaces moving unidirectionally, since any point in space must have a unique arrival time $T$. The former system does not have this restriction, but is somewhat more demanding in terms of computational effort.

This level set approach elegantly avoids the problems associated with marker particle techniques described above. The resulting initial/boundary value problems lend themselves to stable, computationally efficient numerical implementations, which can naturally handle singularities, shocks, weak solutions and even topological changes in the moving surface.

## 4.1. The basic fast marching method

Motivated largely by these ideas, which are due to Sethian [15], a numerical algorithm for tracking the position of a surface was implemented. Due to the unidirectional nature of tree growth, the condition of a unique arrival time function $T(\mathbf{x})$ was not viewed as restrictive, so a boundary value formulation was adopted (see Figure 11). The appropriate partial differential equation for $T$ may be derived as follows. Consider a point $\mathbf{x}(t)$ moving with the surface. Since $T(\mathbf{x})$ is the arrival time of the surface at $\mathbf{x}$, it follows that

$$T\left(\mathbf{x}(t)\right) = t \ .$$

Differentiating with respect to $t$ and substituting for $\dot{\mathbf{x}}(t)$ using equation (1) gives

$$v\mathbf{n} \cdot \nabla T\left(\mathbf{x}(t)\right) = 1 \ .$$

Since $\nabla T$ is normal to the level set of $T$, and hence parallel to the surface outward unit normal $\mathbf{n}$, we have

$$v\left|\nabla T\right| = 1, \tag{12}$$

with the boundary condition that $T = 0$ on the initial location of the surface.

This problem may be solved very efficiently using a fast marching method. The method uses upwind finite differences to propagate information in the appropriate directions. Specifically, the square of equation (12) is discretised as follows:

$$\sum_{m=\{x,y,z\}} \max\left(D_{ijk}^{(m)-}T,\ -D_{ijk}^{(m)+}T,\ 0\right)^2 = v_{ijk}^{-2} \ , \tag{13}$$

where the $ijk$ subscripts indicate the position in the grid, and $D^{(m)}$ is the one-sided finite difference operator in the $m$ direction:

$$D_{ijk}^{(x)\pm}u = \pm\frac{1}{\Delta x}\left(u_{i\pm1,j,k} - u_{i,j,k}\right) \ , \tag{14}$$

(for any $u$) and similarly for $D^{(y)}$ and $D^{(z)}$.

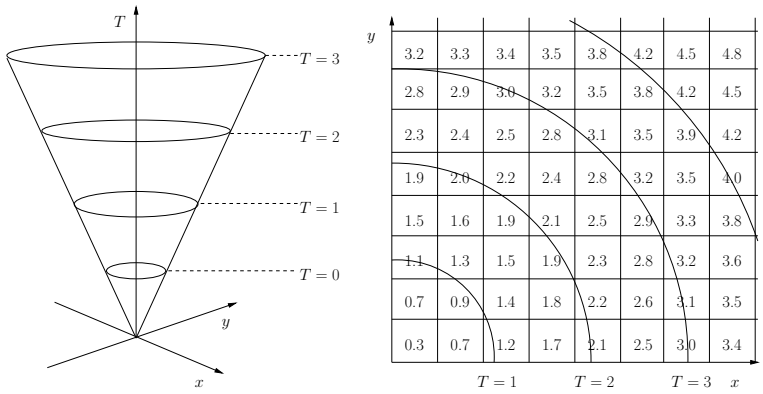


*Figure 11.* Representation of a moving interface using a level set method. $T(x, y)$ is the arrival time of the interface at $(x, y)$ and the position of the interface at time $t$ is the level set $T = t$.

Equation (13) gives a system of quadratic equations for the unknowns $T_{ijk}$. The key to the efficiency of the fast marching method is the surprising observation that, by using the causality relationship between neighbouring grid points, this system may be solved by visiting each grid point *only once*! Because information is always transferred from grid points with smaller values of $T$ to those with larger values, the value of $T_{ijk}$ is only affected by neighbouring grid points with *smaller* values of $T$. Hence, at any stage in the construction of the solution, the grid point with the smallest value of $T$ must be correct and may be fixed. The algorithm for solving the problem thus proceeds as follows (see Figure 12):

1 Approximate the initial surface using a set of grid points. Tag each of these points as 'trial' with an approximation for the correct $T$ value. Tag all other points as 'unknown'.

2 Let $\mathbf{x}_m$ be the grid point with the smallest value of $T$ of all 'trial' grid points.

3 Tag $\mathbf{x}_m$ as 'known'.

4 Using equation (13), compute values of $T$ for all neighbouring points of $\mathbf{x}_m$ that are either 'unknown' or 'trial'; tag any 'unknown' neighbouring points as 'trial'. Repeat steps 2-4 until all grid points are tagged as 'known'.

In practice, the simplest way to achieve step 1 is to set $T = 0$ at all points within a specified region of space and then tag the boundary

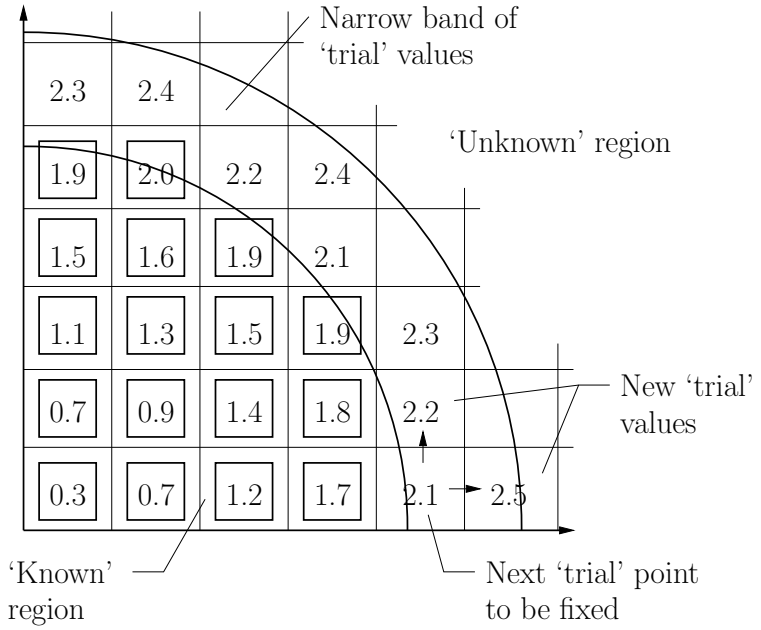


*Figure 12.* The fast marching method for calculating the arrival time function $T(x, y)$. Each grid point is tagged as 'known', 'trial' or 'unknown'. At any given stage in the construction of the solution, the 'trial' point with the smallest value of $T$ is fixed and transferred to the 'known' category; trial $T$ values are then computed for neighbouring 'trial' and 'unknown' points using upwind finite differences.

points of that region as 'trial' and the interior points as 'known'. To obtain a more accurate representation of the boundary data, it may be necessary to construct the signed difference function from the initial surface, setting $T$ to be positive for grid points outside the initial surface, and negative for points inside.

As a further bonus for the efficiency of the method, it is not necessary to search for the grid point $\mathbf{x}_m$ from scratch at each step in the loop. Rather, by maintaining all 'trial' grid points in a heap structure, it is possible to find $\mathbf{x}_m$ in at worst $O(\ln M)$ time, where $M$ is the number of elements in the heap.

It is straightforward to specify the velocity function $v$ as a function of $\mathbf{x}$ and $t$. It is also possible to specify $v$ as a function of curvature as discussed in Section 3. For a two-dimensional problem, the curvature of

the level set curve of $T(x, y)$ may be written:

$$\kappa = \nabla . \frac{\nabla T}{|\nabla T|} = \frac{T_{xx}T_y^2 - 2T_xT_yT_{xy} + T_{yy}T_x^2}{\left(T_x^2 + T_y^2\right)^{\frac{3}{2}}} \ ,$$

whilst the mean curvature of the level surface of $T(x, y, z)$ is:

$$\begin{aligned} \kappa &= \nabla . \frac{\nabla T}{|\nabla T|} \\ &= \Big( \left(T_{yy} + T_{zz}\right)^2 T_x^2 + \left(T_{xx} + T_{zz}\right)^2 T_y^2 + \left(T_{xx} + T_{yy}\right)^2 T_z^2 \\ &\quad -2T_xT_yT_{xy} - 2T_xT_zT_{xz} - 2T_yT_zT_{yz} \Big) \left(T_x^2 + T_y^2 + T_z^2\right)^{-\frac{3}{2}} \ . \end{aligned}$$

Hence $\kappa$ may be calculated using appropriate upwind finite difference approximations for the first and second order derivatives of $T$.

## 4.2. Multicompartment surfaces

What may be more relevant in the case of tree growth is to divide the surface into several compartments (main stem, branch 1, branch 2, etc.), each with its own velocity function.

One means to achieve this computationally is to treat each compartment as a separate surface and evolve it according to the above algorithm. Sethian [15] (§14.7) outlines a general method for evolving multicompartment surfaces according to an "influence matrix", which prescribes the growth rate of each compartment into each other compartment. The situation for tree growth is simpler, since there is assumed to be no growth of one compartment into another; compartments may only grow into free space. A simplified version of Sethian's method may therefore be adopted as follows.

Each compartment $i$ has its own sets of 'known', 'trial' and 'unknown' grid points, with values of the arrival time function $T_{(i)}$ calculated using that compartment's velocity function. At each step in the iteration, let the minimum trial value of $T_{(i)}(\mathbf{x})$ over all $\mathbf{x}$ and all $i$ occur at grid point $\mathbf{x}_m$ and compartment $k$. Then $\mathbf{x}_m$ is moved from the 'trial' to the 'known' set of compartment $k$, so that $T_{(k)}(\mathbf{x}_m)$ is fixed, and is simultaneously added to the 'known' sets of all other compartments $i$ with a $T$ value of $T_{(i)}(\mathbf{x}_m) = \infty$. This method also handles the special case of an inert obstacle (such as a dead branch or external object) around which the tree must grow, as this can be treated as a compartment with a zero velocity function. Accordingly, grid points adjacent to such a compartment will receive trial $T$ values of $\infty$ and hence the compartment will never grow.

The results of implementing this method for the growth of a stem and several branches are shown in Section 7.

## 5. Grain flow

The most advanced works in the literature concerning grain direction are a series of papers by Kramer [6, 8], and a seminal paper is [11]. The idea behind these papers is that growth hormone is transported from the leaves to the roots and the grain attempts to align itself to the local direction of hormone transport. The model produces qualitatively good results, although quantitative comparisons are impossible due to the unavailability of data. Because of this and because hormone transport is beyond the scope of this report, a simplified version of Kramer's model is used. It also produces results that are qualitatively correct.

Assume that grain flows down branches and the stem like an incompressible fluid. The fluid velocity, $\mathbf{g}$, is therefore divergenceless:

$$\nabla \cdot \mathbf{g} = 0 \ . \tag{15}$$

Note that the *magnitude* of $\mathbf{g}$ is unimportant for our purposes: only its *direction* is meaningful. The potential function, $\Phi$ (a scalar), is useful. It is related to $\mathbf{g}$ by

$$\mathbf{g} = \nabla \Phi \ .$$

There are two important examples: a stem containing a dead branch; and, a stem containing a live branch. The details of these are now worked through.

The stem is mapped to a rectangle on the complex plane by a map which simply "unrolls" the stem's surface, and then standard simple solutions of Laplace's equation on the plane are used. These standard solutions do not respect the periodicity of the stem, so that when the solutions are "rolled up" on to the stem again, there will be inaccuracies at the join. However, provided the branch is small in comparison to the stem, these inaccuracies are slight, as will be seen below. The reader should keep in mind that equation (15) is only an approximation, so that these small errors are admissible. It is assumed that the stem and branch are both cylindrical. The generalisation to other shapes will become apparent: a different map to the complex plane should be used. Once again, given that the incompressible fluid approach is only an approximation which produces qualitatively correct results, it may not be necessary to construct a highly accurate map until such time as experimental data become available.

## 5.1. Stem containing dead branch

In this case the stem-grain does not enter the branch at all, and the branch acts as a barrier to the 'flow' of the grain on the stem. The branch-grain simply runs axially, or possibly helically from end to end, so it is the stem's grain that is nontrivial.

Coordinatise the stem's surface (radius $r_{\rm s}$) with cylindrical polar coordinates $(\phi, h)$. Here $\phi \in (-\pi, \pi)$. Because it is easy to solve equation (15) on the complex plane, map the stem to the plane using

$$y = h \quad \text{and} \quad x = r_{\rm s}\phi \ .$$

This map is shown in Figure 13.

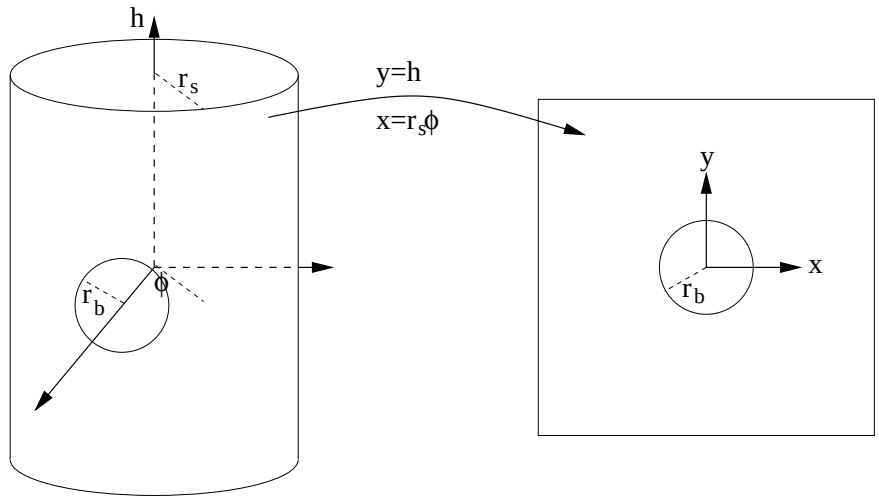


*Figure 13.* Map from stem of radius $r_{\rm s}$ to the complex plane. The circle of radius $r_b$ represents the base of a dead branch. The map is simply cutting open the stem's surface and laying it flat.

Introduce the complex quantity $z$:

$$z = x + iy = re^{i\theta} \ .$$

Let the branch have radius $r_{\rm b}$. There must be no normal flow on the circle $|z| = r_b$. It is well-known that the solution for the potential function is [5]

$$\Phi = i\left(z - \frac{r_{\rm b}^2}{z}\right) \ .$$

The velocity, $\mathbf{g} = (\mathbf{g}_x, \mathbf{g}_y)$, given by the formula $\mathbf{g}_x - i\mathbf{g}_y = \mathrm{d}\Phi/\mathrm{d}z$, is therefore

$$\mathbf{g}_x = \frac{r_\mathrm{b}^2}{r^2}\sin 2\theta = \frac{2xyr_\mathrm{b}^2}{(x^2+y^2)^2} \tag{16}$$

and

$$\mathbf{g}_y = -1 - \frac{r_\mathrm{b}^2}{r^2}\cos 2\theta = -1 - \frac{(x^2-y^2)r_\mathrm{b}^2}{(x^2+y^2)^2}\ . \tag{17}$$

This is plotted in Figure 14, where it can be seen that the grain flows realistically around the dead branch.

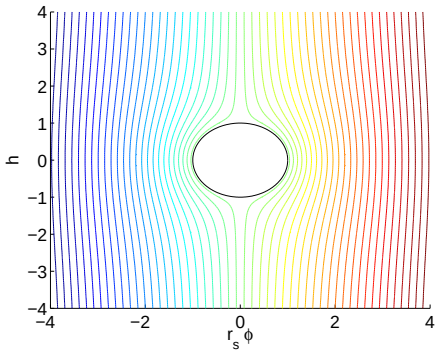


*Figure 14.* Grain pattern on the surface of the main stem around a dead branch for $r_\mathrm{b} = 1$. No grain enters or leaves the branch.

Mapping back to the stem (with $\mathbf{g} = \mathbf{g}_h\hat{k} + \mathbf{g}_\phi\hat{\phi}$ where $\hat{k}$ is the unit vector in the $h$ direction and $\hat{\phi}$ is the unit vector in the $\phi$ direction) gives

$$\mathbf{g}_h = -1 + \frac{(h^2 - r_\mathrm{s}^2\phi^2)r_\mathrm{b}^2}{(h^2+r_\mathrm{s}^2\phi^2)^2} \quad \text{and} \quad \mathbf{g}_\phi = \frac{2r_\mathrm{b}^2 r_\mathrm{s} h\phi}{(h^2+r_\mathrm{s}^2\phi^2)^2}\ .$$

Alternatively, this can be expressed in a Cartesian frame (using $\mathbf{g} = \mathbf{g}_X\hat{\imath} + \mathbf{g}_Y\hat{\jmath} + \mathbf{g}_h\hat{k}$ in the usual notation) with

$$\mathbf{g}_X = -\mathbf{g}_\phi \sin\phi \quad \text{and} \quad \mathbf{g}_Y = \mathbf{g}_\phi\cos\phi\ .$$

It may be noticed that $\mathbf{g}(\phi = -\pi) \neq \mathbf{g}(\phi = \pi)$. As mentioned above, this is means that as the rectangular domain is "rolled up" onto the cylindrical stem, there will be a discontinuity in the solution for the grain vector at the join ($\phi = \pm\pi$). However, if $r_\mathrm{s} \gg r_\mathrm{b}$, the solution given is close to periodic and the discrepancy is small. If, in future, a perfectly periodic solution is required, then $\Phi$ should be modified so that it is periodic under $x \to x + 2\pi r_\mathrm{s}$.

## 5.2. Stem with live branch

A similar approach can be taken here, although the mapping is more complicated. Again, coordinatise the stem's surface with $(\phi, h)$. Similarly, coordinatise the branch's surface with $(\phi_\mathrm{b}, h_\mathrm{b})$, where $\phi_b = 0$ on the top of the branch and $h_\mathrm{b} = 0$ at its base. Then map to the complex plane ($z = x + iy = re^{i\theta}$) using

$$y = h \ , \quad x = r_\mathrm{s}\phi \ , \quad r = r_\mathrm{b}e^{-h_\mathrm{b}} \ , \quad \theta = \phi_\mathrm{b} + \pi/2 \ ,$$

where the first two map the stem (the same as in the previous section) and the final two map the branch. The map for the branch is shown in Figure 15.

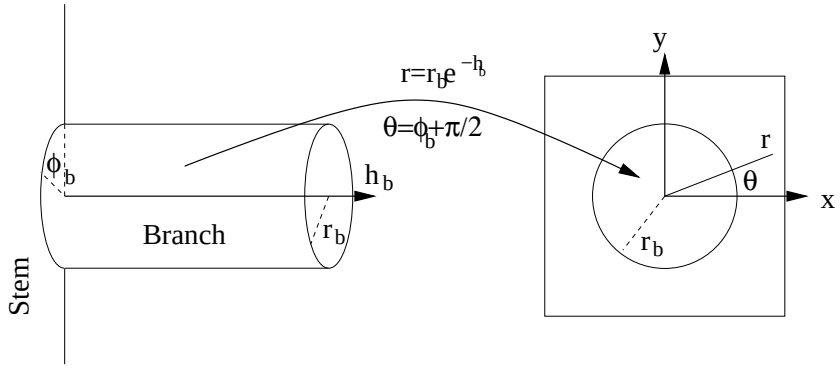


*Figure 15.* Map of a branch of radius $r_\mathrm{b}$, coordinatised by cylindrical polar coordinates $(\phi_\mathrm{b}, h_\mathrm{b})$ to a disc on the complex plane. The map is simply squashing the branch along its axis, with the circle at $h_\mathrm{b} = \infty$ being mapped to the origin.

The branch acts as a point source in a flow field which has $\mathbf{g}_y = -1$ asymptotically at $r \to \infty$. The solution for the potential function is again well known [5], and it is

$$\Phi = iz + r_\mathrm{b} \log z \ .$$

Differentiation yields

$$\mathbf{g}_x = \frac{r_\mathrm{b}}{r}\cos\theta = \frac{r_\mathrm{b}x}{x^2+y^2} \quad \text{and} \quad \mathbf{g}_y = -1 + \frac{r_\mathrm{b}}{r}\sin\theta = -1 + \frac{r_\mathrm{b}y}{x^2+y^2} \ . \quad (18)$$

The potential has been constructed so that there is no flow from the stem down into the branch and there is no flow from the top of the branch up into the stem.

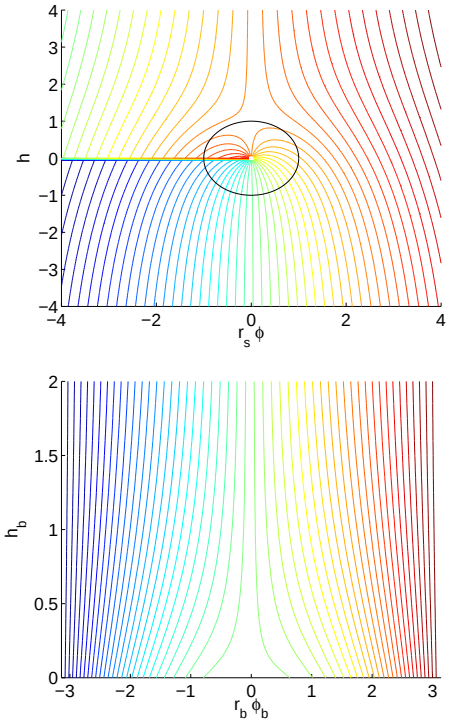


*Figure 16.* Grain pattern: (a) on the surface of the main stem around a live branch; (b) on the branch ($r_\mathrm{b} = 1$). Grain 'flows' out of the branch and down the stem, but no grain enters the branch from above.

This solution can be mapped back to the stem-branch system. On the stem:

$$\mathbf{g}_h = -1 + \frac{r_\mathrm{b} h}{h^2 + r_\mathrm{s}^2 \phi^2} \quad \text{and} \quad \mathbf{g}_\phi = \frac{r_\mathrm{s} r_\mathrm{b} \phi}{h^2 + r_\mathrm{s}^2 \phi^2} \ .$$

On the branch (with $\mathbf{g} = \mathbf{g}_{h_\mathrm{b}} \hat{k}_b + \mathbf{g}_{\phi_\mathrm{b}} \hat{\phi}_b$, where $\hat{k}_b$ is the unit vector along the branch's axis, and $\hat{\phi}_b$ is the unit vector in the angular direction around the axis):

$$\mathbf{g}_{h_\mathrm{b}} = -e^{h_\mathrm{b}} + \cos\phi_\mathrm{b} \quad \text{and} \quad \mathbf{g}_{\phi_\mathrm{b}} = \sin\phi_\mathrm{b} \ .$$

Recall that $\phi_b = 0$ is at the top surface of the branch. As $h_\mathrm{b} \to \infty$, $\mathbf{g}/|\mathbf{g}| \to -\hat{k}_b$, which means that, a long way from the stem–branch junction, the grain flows parallel to the main axis of the branch, as expected. These results may be expressed in a Cartesian frame using the same formulae as the previous section. The solution is plotted in Figure 16.

## 6. Fast marching method for anisotropic, multicompartment surfaces

In this section, a method is outlined for extending the fast marching method described in Section 4 to anisotropic surface growth by incorporating the grain direction on the surface. To achieve this, some simple assumptions are made:

1 The grain direction field $\mathbf{g}(\Gamma)$ on the initial surface $\Gamma$,

$$\Gamma = \left\{\mathbf{r} : T_{(i)}(\mathbf{r}) = 0 \text{ for some } i\right\} \ ,$$

is known.

2 When a grid point $\mathbf{r}_m$ enters the 'known' set of compartment $i$, its grain direction is related to that of its parent point $\mathbf{r}_p$, defined as the point with the *lowest* value of $T_{(i)}$ of all neighbouring points in the 'known' set of compartment $i$.

3 The grain vector $\mathbf{g}(\mathbf{r}_m)$ is calculated according to the following rules, which give three equations in three unknowns:

   (a) The grain is tangent to the surface at $\mathbf{r}_m$, that is; $\mathbf{g}(\mathbf{r}_m).\nabla T(\mathbf{r}_m) = 0$.

   (b) The grain vector has the same norm as that of its parent: $|\mathbf{g}(\mathbf{r}_m)| = |\mathbf{g}(\mathbf{r}_p)|$.

   (c) The scalar product of the grain vectors at $\mathbf{r}_m$ and $\mathbf{r}_p$ is maximal: $\mathbf{g}(\mathbf{r}_m).\mathbf{g}(\mathbf{r}_p) = \max_{\mathbf{w}} \mathbf{w}.\mathbf{g}(\mathbf{r}_p)$, where $\mathbf{w}$ is a vector satisfying constraints (a) and (b).

In general, this will result in new grain vectors being very similar to the parent vectors, with a slight readjustment if necessary to ensure that the grain remains tangent to the surface.

It would be possible to modify this method to model spiral grain changing direction over time. This could be accomplished by specifying a rate of rotation of the grain vector about the surface normal. This rate may depend on the position on the tree surface and on time.

## 7. Visualisation

The output from the fast marching method is simply an array of arrival times. These can be efficiently visualised using MATLAB's `isosurface` function, which plots the level set of a three-dimensional function. For example, the surface at time $t > 0$ (i.e. the level set $T(x, y, z) = t$) may be plotted using the command

```
>> isosurface(T,t).
```

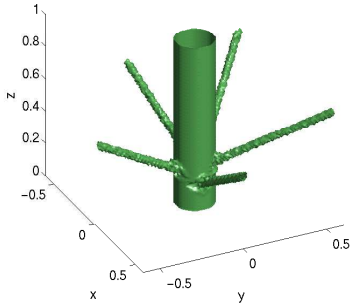


(a)

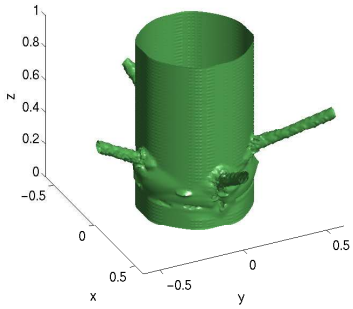


(b)

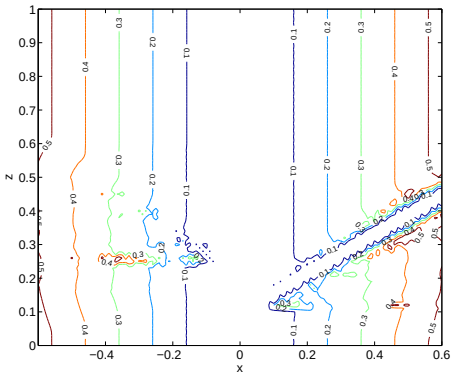


(c)

*Figure 17.* Growth of a stem and 5 branches: (a) $t = 0.05$; (b) $t = 0.25$; (c) contour plot of $T$ on a vertical cross section through the tree. The initial configuration is given in Table 1; the velocity is constant, but main stem velocity is different to the velocity of the branches.

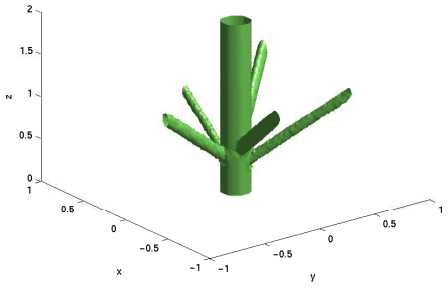


(a)

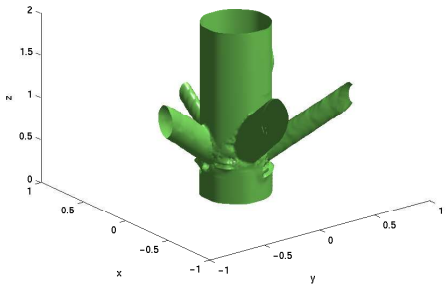


(b)

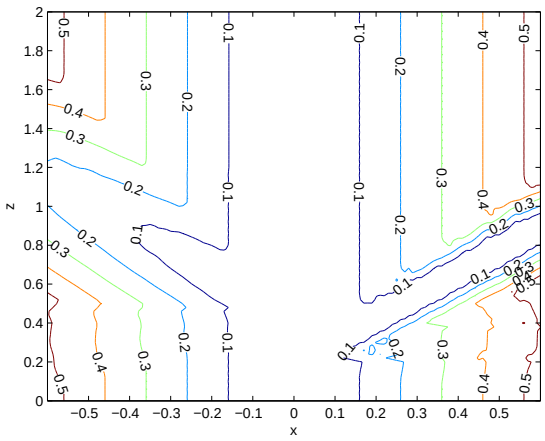


(c)

*Figure 18.* Growth of the tree with variable growth rates: (a) $t = 0.05$; (b) $t = 0.20$; (c) contour plot of $T$ on a vertical cross section through the tree. The growth rate is different for each compartment (main stem and branches 1-5), as shown in Table 1. The growth rate for all compartments is decreasing with time: $v = v_0 e^{-kt}$.

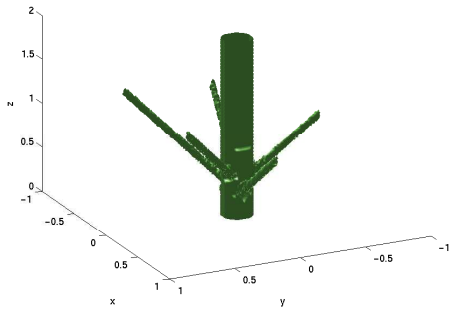


(a)

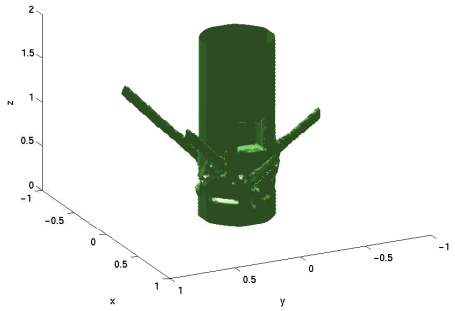


(b)

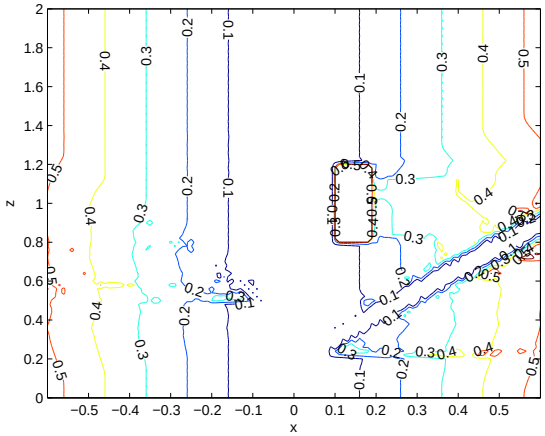


(c)

*Figure 19.* Growth of the tree around an obstacle: (a) $t = 0.05$; (b) $t = 0.25$; (c) contour plot of $T$ on a vertical cross section through the tree. The obstacle is a cuboid centred at $x = 0.15$, $y = 0$, $z = 0.5$. The velocity is constant as in Figure 17.

| Compartment | $h$ (mm) | $d$ (mm) | $\theta$ (°) | $\phi$ (°) | $v_0$ |
|---|---|---|---|---|---|
| S | 0 | 13.5 | | 0 | 6.0 |
| B1 | 500 | 5.0 | 0.0 | 60 | 1.0 |
| B2 | 503 | 5.0 | 137.5 | 60 | 1.5 |
| B3 | 506 | 5.0 | 275.0 | 60 | 2.0 |
| B4 | 509 | 5.0 | 412.5 | 60 | 2.5 |
| B5 | 512 | 5.0 | 550.0 | 60 | 3.0 |

*Table 1.* Initial configuration of the tree surface, consisting of 6 cylindrical compartments: the main stem (S) and 5 branches (B). $h$ is the height of the base of the cylinder; $d$ is the diameter of the cylinder; $\theta$ and $\phi$ are the angles of the main axis of the cylinder with the horizontal ($x$) axis and the vertical ($z$) axis respectively; $v_0$ parameterises the relative growth rate of the compartment. These values of $\theta$ can be found in [12], and the other measurements are typical of pinus radiata.

A run of the fast marching method was made with parameters listed in Table 1. This models a situation where five branches form a cluster around a main stem, and all branches grow at the same rate. The results are visualised in Figure 17.

Figure 18 shows the case where the growth rate is exponentially decreasing with time: $v = v_0 e^{-kt}$. Additionally, the initial growth rate $v_0$ is different for all compartments (the main stem and each of the five branches), as shown in Table 1.

Figure 19 shows the growth of a stem around an obstacle. Here the growth velocity is constant and independent of curvature (as in Figure 17). The "knuckles" seen in Figure 5 are evident.

## 8. Conclusions

Ensis brought a problem concerning tree growth to MISG2006: they wanted participants to develop a robust framework for describing growing surfaces which may be anisotropic. During the course of MISG2006, the fast marching method of Sethian [15] was identified as being suitable since it was numerically stable under any physically reasonable local evolution law.

The Ensis representatives presented MISG2006 with data concerning tree growth which loosely defined the range of evolution laws typical for this type of problem. These data are discussed in Section 2. In particular, the growth is time-dependent; branches often die and act as obstacles to the stem's growth; there are often concave regions around a branch–stem junction; there are often 'bumps' of enhanced growth when wood impinges on obstacles or branches; and grain runs from leaves to roots rather like an incompressible fluid.

In the mathematical literature, growth of surfaces is often driven by the local curvature. It was argued that this is possibly not relevant for tree growth. However, analytical studies of curvature-driven growth were made in Section 3. Explicit formulae for the curvature and torsion of a space curve, and the curvatures of 2D surfaces were presented. Formulae concerning the evolution of a curve in two dimensions with an arbitrary evolution law were derived: the evolution of distances along the curve (the 'curve metric'); the evolution of the curvature; and the evolution of the average value of the magnitude of curvature (the 'total variation'), were written. An example model of curvature-driven growth of a tree impinging upon a barrier was solved explicitly, but it did not display a 'bump' of enhanced growth, possibly due to the simplifications in the analysis. An example model of curvature- and hormone-driven growth was also solved analytically, and this did display the 'bump' of enhanced growth around the region of the obstacle, because the model assumed that growth hormone was released in this region.

In Section 4 the fast marching method for an isotropic surface was described. It was explained why this is superior to the classical marker-tracking algorithms because of instabilities arising from marker particles growing into one another. The fast marching method represents the surface as a level set of a time-of-arrival function. The evolution law was derived, and an efficient finite-differencing scheme was introduced (due to Sethian [15]), which naturally leads to an algorithm for solving the problem. The extension to 'multicompartment surfaces', which have different growth rates ascribed to different regions (representing stem, branches and obstacles, for instance) is due to Sethian too, but a simplification is possible since in the case of tree growth the compartments remain disjoint (stems do not grow in obstacles, etc). This simplified algorithm was described.

Grain patterns were explored in Section 5. The work follows Kramer [6, 8], who proposes that grain patterns may be reproduced by modelling the grain as flow lines of an incompressible fluid. Analytic results for incompressible fluid flow are available and it was shown how to map these from the complex plane to the surface of a stem/branch for two model cases: a stem containing a dead branch; and a stem with a live branch.

The fast marching method can be extended to include anisotropic surfaces, once the evolution law concerning the vector(s) describing the anisotropy (the grain evolution laws) are given. The framework was described in Section 6. Since there were no data concerning the time evolution of grain directions, an algorithm was given for the simplest case, which was when the grain direction evolved minimally in that it attempted to align itself with previously-formed grain.

Finally, it was described, in Section 7, that the results may be efficiently visualised using MATLAB. Some test situations were visualised: a stem with a cluster of 5 branches; the growth around an obstacle with constant growth velocity; and a combination of these two with various different growth rates for the stem and branches.

**Acknowledgements**

The project moderators, Jo Mann, Mike Plank and Andy Wilkins, thank the representatives from Ensis, Jenny Grace and Jonathan Harrington, for helping with the problem's solutions as well as providing a lot of background information. Participants of the MISG did the majority of the work. In particular we would like to thank Duangkamon Baowan, Ron Begg, Phil Broadbridge, Vivien Challis, Grant Cox, Glenn Fulford, Tamsyn Hilder, Graeme Hocking, Peter Howell, Karen Lewis, Kim McKelvey, Robert McKibbin, and Bruce van-Brunt.

**Appendix: Mathematical notation**

| | |
|---|---|
| $a$ | term in the growth velocity $v$ independent of curvature ($v = a + b\kappa$) |
| $a$ | arclength along a space curve. *Only* in Sections 3.2.2 and 3.2.4 |
| $A$ | the surface area of the tree |
| $b$ | coefficient of the linear term in the growth velocity $v$ (i.e. $v = a + b\kappa$) |
| $\tilde{b}$ | defined in $v = a(1 + \tilde{b}\kappa)$ |
| $\mathbf{B}$ | unit binormal vector to a space curve |
| $\mathbf{B}'$ | derivative of $\mathbf{B}$ with respect to $\xi$ |
| $\beta(\xi)$ | a family of curves which follow the normals to $\gamma(t)$ |
| $C$ | $C = C(x,t)$ is the concentration of hormone at point $x$ at time $t$. |
| $d$ | diameter of a cylindrical stem or branch |
| $D$ | diffusivity constant of hormone |
| $D^m_{ijk}$ | one-sided finite difference operators in direction $m$ at point $(i,j,k)$ in 3-space. Defined in equation (14) |
| $E$ | measure of distance along a space curve (the "curve metric"): see equation (3) |
| $F$ | A measure of distance along a space curve, see equation (3) |
| $\phi$ | The slope angle of a space curve: see Figure 8. In Section 3 |
| $\phi$ | level set function in Section 4 |
| $\phi$ | angular coordinate in Section 5 |
| $\phi$ | angular coordinate of the branches in Section 7 |
| $\phi_b$ | angular coordinate on the branch in Section 5 |
| $\Phi$ | potential function for grain flow, defined by $\mathbf{g} = \nabla\Phi$ |
| $\mathbf{g}$ | vector pointing along the direction of the grain |
| $G$ | A measure of temporal distance along a space curve, see equation (3) |
| $\gamma(t)$ | a family of space curves: $\gamma(0)$ is the space curve at time 0, and so on |
| $\Gamma$ | the initial surface of a tree |
| $h$ | height coordinate along the stem in Section 5.1 |
| $h$ | height of the branches along the stem in Section 7 |
| $h_b$ | height coordinate along the branch in Section 5.2 |
| $_{(i)}$ | (subscript $(i)$) labels the compartment $i$. |

| | |
|---|---|
| $k$ | exponential decay parameter in the growth velocity $v = v_0 e^{-kt}$ |
| $k_1$ $k_2$ | principal curvatures of a surface |
| $\kappa$ | the curvature at a point on the tree's surface<br>also, curvature of a space curve at a point |
| $L$ | length measured by an ant running on a surface |
| $\Lambda$ | The total variation of a curve $\gamma(t)$, defined in equation (8) |
| $\mathbf{n}$ | unit normal at a point on the tree's surface |
| $\mathbf{N}$ | unit normal vector to a space curve |
| $\mathbf{N}'$ | derivative of $\mathbf{N}$ with respect to $\xi$ |
| $\nabla$ | the derivative $\nabla = (\partial/\partial x, \partial/\partial y, \partial/\partial z)$ in 3-space |
| $q_0$ | arbitrary proportionality constant in Gaussian approximation to $C$. |
| $r_\mathrm{b}$ | radius of a branch |
| $r_\mathrm{s}$ | radius of the stem |
| $r$ | radial coordinate on the complex plane: $z = re^{i\theta}$ |
| $\mathbf{r}$ | coordinates of a point on the tree's surface |
| $\mathbf{r}'$ $\mathbf{r}''$ | derivatives of $\mathbf{r}$ with respect to $\xi$. |
| $\mathbf{r}_m$ | coordinates of a point on the tree's surface with parent $\mathbf{r}_p$ |
| $\mathbf{r}_p$ | coordinates of a point on the tree's surface which has daughter $\mathbf{r}_m$ |
| $R^3$ | 3-dimensional space (Euclidean) |
| $s$ | arclength. Thus d$s$ is arclength along an infinitesimally-long curve |
| $t$ | time. Also, d$t$ is an infinitesimal increment of $t$ |
| $_t$ | (subscript $t$) indicates a derivative with respect to $t$. E.g. $x_t = \partial x/\partial t$ |
| $T$ | time of arrival function $T = T(\mathbf{x})$ in the fast marching method |
| $T_{ijk}$ | time of arrival at point $(i, j, k)$ in 3-space |
| $\mathbf{T}$ | unit tangent vector to a space curve |
| $\mathbf{T}'$ | derivative of $\mathbf{T}$ with respect to $\xi$ |
| $\tau$ | torsion of a space curve at a point |
| $\theta$ | angular coordinate on the complex plane: $z = re^{i\theta}$ in Section 5 |
| $\theta$ | angular coordinate of the branches in Section 7 |
| $u$ | $u(x,t) = y(x,t) + x$ in Section 3.2.6 |
| $v$ | velocity function controlling growth rate |
| $v_\mathrm{branch}$ | velocity function controlling the growth rate of the branch |
| $v_\mathrm{stem}$ | velocity function controlling the growth rate of the stem |
| $\mathbf{v}$ | an arbitrary unit tangent vector to a surface |
| $x$ | In 2D we can decompose $\mathbf{r}$ into Cartesian coordinates: $\mathbf{r} = (x, y)$ |
| $x$ | Cartesian coordinate in Section 5. Related to the complex coordinate $z$ by $z = x + iy$ |
| $\mathbf{x}$ | coordinate point in 3D in the fast marching method |
| $\mathbf{x}_m$ | 'trial' grid point with smallest value of $T$. |
| $_x$ | (subscript $x$) denotes differentiation with respect to $x$.<br>*except* in equations (16), (17) and (18) where it denotes components of $\mathbf{g}$ in the complex plane |
| $\xi$ | arbitrary parameter which varies monotonically along a space curve. Although not necessary, $\xi$ may be chosen to be arclength, in which case various formulae simplify since $\lvert\mathbf{r}'\rvert = 1$.<br>Also, d$\xi$ is an infinitesimal increment of $\xi$ |
| $\xi_0$ $\xi_1$ | label the beginning and end of a space curve |
| $_\xi$ | (subscript $\xi$) indicates a derivative with respect to $\xi$. E.g. $x_t = \partial x/\partial \xi$ |
| $y$ | In 2D we can decompose $\mathbf{r}$ into Cartesian coordinates: $\mathbf{r} = (x, y)$ |

| | |
|---|---|
| $y$ | Cartesian coordinate in Section 5. Related to the complex coordinate $z$ by $z = x + iy$ |
| $_y$ | (subscript $y$) denotes differentiation with respect to $y$, *except* in equations (16) and (17) and (18) where it denotes components of $\mathbf{g}$ in the complex plane |
| $z$ | Complex coordinate |

# References


[1] Broadbridge, P., "Exact solvability of the Mullins nonlinear diffusion model of groove development", *J. Math. Phys.*, **30** (1989), pp. 1648–1651.

[2] Grace, J., private communication (to be published).

[3] Grace, J., *New Zealand J. Forestry Sci.*, **28** (1998), pp. 182–194.

[4] Grace, J., *New Zealand J. Forestry Sci.*, **29** (1999), pp. 391–408.

[5] Hildebrand, F. B. (1976). Advanced Calculus for Applications. 2nd ed. Prentice-Hall, New Jersey. Section 11.6.

[6] Kramer, E. M., "A mathematical model of auxin-mediated radial growth in trees", *J. Theor. Biol.*, **208** (2001), pp. 387-397.

[7] Kramer, E.M., "A mathematical model of pattern formation in the vascular cambium of trees", *J. Theor. Biol.*, **216** (2002), pp. 147–158.

[8] Kramer, E. M. and Borkowski, M. H., "Wood grain patterns at branch junctions: modelling and implications", *Trees*, **18** (2004), pp. 493-500.

[9] Mattheck, C., *Design in Nature: learning from trees*, Springer-Verlag, Berlin, New York, (1998).

[10] Perttunen J., Sievanen R. and Nikinmaa E., "LIGNUM: a model combining the structure and the functioning of trees", *Ecol. Modelling*, **108** (1998), pp. 189–198.

[11] Philips, G. E., Bodig, J., Goodman, J. R., "Flow-grain analogy", *Wood Sci.*, **14** (1981), pp. 55–64.

[12] Pont, D., "Use of phyllotaxis to predict arrangement and size of branches in Pinus radiata", *New Zealand J. Forestry Sci.*, **31** (2001), pp. 247–262.

[13] Shashkin, A. V., Fritts, H. C., Downes, G. M., " A process model of cambial activity and ring structure in conifers using daily climatic data", (2001), http://www.ltrr.arizona.edu/webhome/hal/halmodel.html

[14] Sethian, J. A., "Curvature and Evolution of Fronts", *Comm. Math. Phys.*, **101** (1985), pp. 487–499.

[15] Sethian, J. A., *Level set methods and fast marching methods. Evolving interfaces in computational geometry, fluid mechanics, computer vision and materials science*, 2nd Ed., Cambridge University Press, Cambridge, (1999).

[16] Shigo, A. L., "How tree branches are attached to trunks", *Canadian J. Botany*, **63** (1985), pp. 1391–1401.

[17] Shigo, A. L., *A new tree biology dictionary: terms, topics, and treatments for trees and their problems and proper care*, Shigo and Trees Associates, Durham NH, (1986).

[18] Shigo, A. L., *Tree basics*, Shigo and Trees Associates, Durham NH, (1998).

[19] Turing, A., "The chemical basis of morphogenesis", *Phil. Trans. Roy. Soc. B*, **237** (1952), pp. 37–72.

[20] http://en.wikipedia.org/wiki/Curvature.

[21] http://en.wikipedia.org/wiki/Frenet-Serret_formulas.

[22] http://en.wikipedia.org/wiki/Mean_curvature.